Polymer Testing 149 (2025) 108858

Contents lists available at ScienceDirect

Polymer Testing

journal homepage: www.elsevier.com/locate/polytest

Compression and torsion testing for elastic moduli and Poisson's ratio characterization in silicone rubber samples with varying shape factors

Julen Cortazar-Noguerol [a,*], Fernando Cortés [a], Iker Agirre-Olabide [b], María Jesús Elejabarrieta [a]

[a] Department of Mechanics, Design and Industrial Management, University of Deusto, Avda. de las Universidades 24, 48007, Bilbao, Spain
[b] Engineering Department, Public University of Navarre (UPNA), Arrosadia Campus, 31006, Pamplona, Spain

ARTICLE INFO

Keywords:
Compression tests
Torsional rheometry
Shape factor effects
Correction models
Poisson's ratio
Elastomeric materials

ABSTRACT

Elastomeric materials, such as silicone rubber, are widely used in engineering applications due to their high deformability and viscoelastic properties. Under quasistatic regime and small deformations their behavior can be considered purely elastic and can be characterized by the elastic modulus, shear modulus, and Poisson's ratio, which are interrelated in isotropic materials. Although standard methodologies exist for determining these properties, experimental measurements are known to be affected by the geometry of the tested samples. The influence of sample geometry on compressive modulus measurements is well understood, however, its effect on shear modulus measurements is less explored. This study investigates how the dimensions of cylindrical samples influence the experimental determination of both the compressive and shear moduli and, consequently, Poisson's ratio. Compression and torsion tests are performed on silicone rubber samples of varying diameters and lengths using a dynamic mechanical analyzer and a rheometer respectively. The results confirm that both the compressive and shear moduli are affected by sample geometry, leading to unrealistic values of Poisson's ratio. To account for these effects, a correction model is proposed for shear modulus measurements, complementing existing corrections for compressive tests. The model successfully describes experimental trends and provides a more reliable estimation of Poisson's ratio, aligning with theoretical expectations for nearly incompressible elastomers. These findings emphasize the importance of considering geometric effects in compressive and torsion tests and provide a framework for improving the accuracy of mechanical characterization in elastomeric materials.

1. Introduction

Elastomeric materials, such as silicone rubber, are widely used in engineering applications due to their high deformability, durability, and viscoelastic properties. These materials usually exhibit time-dependent mechanical responses that combine both elastic and viscous effects [1–3]. However, under quasistatic regime (low strain rates) and small deformations, their behavior can be approximated as purely elastic [4,5]. In such cases, the mechanical response is typically characterized by their elastic properties, as the elastic modulus, shear modulus, and Poisson's ratio, which describe their response under different loading conditions [4]. In isotropic materials, these three properties are interrelated, meaning that knowing any two allows for the calculation of the third. Accurate characterization of these properties is essential for the application of numerical methods, which are commonly used to predict the mechanical response of elastomeric components in engineering applications [6].

Techniques using strain gauges [7] or precise volume changes [8] have traditionally been used to determine strain in the transverse axis, allowing for the calculation of Poisson's ratio. However, modern experiments predominantly rely on digital image correlation (DIC) due to its higher accuracy and ability to provide full-field strain measurements. In tensile tests combined with DIC, uniaxial stress is applied to a standardized sample, and the resulting strain is measured along both the loading and transverse directions. By capturing the strain distribution with DIC, Poisson's ratio can be directly determined alongside the elastic modulus, providing a comprehensive characterization of the material's mechanical response [9–11]. However, this method requires specialized cameras and is limited to quasi-static stress-strain measurements. Moreover, the most common application case for elastomers is

* Corresponding author.
E-mail address: j.cortazar@deusto.es (J. Cortazar-Noguerol).

https://doi.org/10.1016/j.polymertesting.2025.108858
Received 28 February 2025; Received in revised form 7 May 2025; Accepted 15 May 2025
Available online 15 May 2025

under compression [4].

The determination of the elastic modulus through compression tests carries its own difficulties. It is well-known and established that the geometry of the sample influences the measurements, as wider samples exhibit higher apparent stiffness, and existing models can address this issue [5,12,13].

Similarly, the determination of the shear modulus presents its own set of challenges. It is commonly obtained through torsion tests [14] or dynamic mechanical analysis using shear loading configurations [15]. Rheometric torsion tests offer a straightforward test configuration. However, conventional rheometric torsion tests are typically conducted on thin film-like cylindrical samples [16,17], which originates from rheometric testing of resins and other types of soft polymers, as indicated in the standard ISO 3219-2 [18]. Meanwhile, the effect of the thickness of the cylindrical samples in the obtained results have been reported [19]. Even though there is no consensus regarding the possible reasons for this effect, nor an in-depth study to address it, multiple references point to wall slippage in the parallel plate configuration [20–22] and the effect of the normal force applied to the sample. Borin et al. [19], in particular, studied the effect of the length of the sample in the accuracy of rheometric torsion testing. They concluded that rod-like samples lead to better results in terms of repeatability and physical meaning, considering they achieve a plausible value for Poisson's ratio of the tested material, and determined that measuring the shear modulus of disc-like samples lead to lower-than-expected values.

Lastly, determining Poisson's ratio experimentally through the compressive and shear moduli remains a challenge. Given the apparent compressive modulus is overestimated [4,5] and the apparent shear modulus is underestimated [19], the results exceed the physical limit of 0.5. Nevertheless, Pal and Bhattacharyya [15] achieved a feasible Poisson's ratio value through tension and simple shear tests, validating their results with the DIC-based approach mentioned above. Although promising, their technique does not allow for the testing of the same samples in both compressive and torsion mode and require specialized imaging equipment.

In summary, the influence of sample geometry on the measured compressive modulus of elastomers is well understood, with established models available to correct shape factor effects. However, in torsion tests, where the shear modulus is determined, the impact of sample geometry remains an open question, with existing studies focusing primarily on sample thickness while neglecting the effect of diameter [19]. Since the ratio between diameter and length is what influences compression test results, it is reasonable to expect a similar dependency in torsion tests. The lack of a correction model for torsion tests introduces uncertainty in the determination of the shear modulus and, consequently, Poisson's ratio, as both parameters are interdependent in isotropic materials. To address this gap, this study proposes and validates a model that accounts for geometric effects in torsion tests while applying a well-established correction for compression tests. The compressive and shear moduli are measured on the same cylindrical silicone rubber samples to ensure direct comparability, minimizing variability due to material inconsistencies. This approach enables the accurate determination of both moduli, leading to a reliable calculation of Poisson's ratio across different shape factors.

The structure of this paper is as follows. Section 2 outlines the theoretical framework, including the constitutive equations for linear elasticity and the concept of shape factor. Section 3 describes the experimental setup, covering sample preparation, testing equipment, and measurement procedures. Section 4 presents and discusses the experimental data obtained from compressive and torsion tests. Section 5 introduces the proposed models, their validation through curve fitting, and the analysis of the results. Finally, Section 6 provides the main conclusions.

2. Theoretical framework

Although elastomeric materials are intrinsically viscoelastic and may exhibit nonlinear behavior under large deformations or high deformation rates, the present study focuses on conditions where such effects are minimal, i.e. under quasistatic regime and low deformations. Under these circumstances, the mechanical response of the material can be accurately approximated by linear isotropic elasticity [4,5]. Based on this assumption, the theoretical framework presented below is restricted to linear elastic behavior.

Throughout this work, both the samples and the performed tests exhibit cylindrical symmetry. On the one hand, the compressive stress-strain tests are defined by the applied force F and the resultant displacement δ (see Fig. 1 (a)). Assuming the tests are quasistatic and within the linear elasticity region of an isotropic material, the relationship between this two magnitudes is given by [4]

$$F = \frac{EA}{L}\delta, \tag{1}$$

where E is the elastic modulus of the tested material, $A = \pi d^2/4$ is the cross-sectional area of the cylindrical sample of diameter d and L is the length (or height).

By defining the engineering stress $\sigma = F/A$ and strain $\varepsilon = \delta/L$, Eq. (1) can be written as

$$\sigma = E\varepsilon. \tag{2}$$

On the other hand, the torsion tests in cylinders are defined by the applied torque M and the resultant angular displacement θ (see Fig. 1 (b)). Under the same conditions as the compressive tests (quasistatic and linear regime), the relationship between these magnitudes is given by

$$M = \frac{G\pi d^4}{32L}\theta, \tag{3}$$

where G is the shear modulus of the tested material. In this case, the maximum shear stress (at the edge of the cylinder) $\tau = 16M/\pi d^3$ and shear strain $\gamma = d\theta/2L$ can be defined so Eq. (3) is reduced to

$$\tau = G\gamma. \tag{4}$$

Both the presented moduli (elastic and shear), are related in isotropic materials through Poisson's ratio such that

$$G = \frac{E}{2(1+\nu)}, \tag{5}$$

where ν represents Poisson's ratio of the material. This way, by measuring two of the three elastic properties presented in Eq. (5), the third can be determined.

However, the experimental determination of the elastic and shear moduli is not straightforward. It is widely known that the experimental compressive modulus depends on the size of the sample, in particular, in

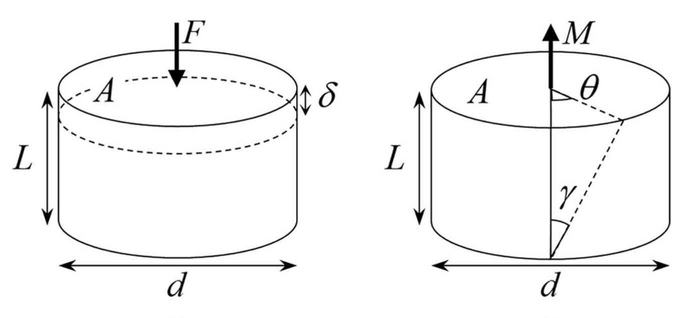

Fig. 1. Deformation modes diagram in (a) compressive and (b) torsion tests for cylindrical samples.

its shape factor (SF) [12,23]. The SF of a sample S is defined as the ratio between the loaded area and the free to bulge area, which, in the case of a cylinder is

$$S = \frac{\pi d^2}{4\pi d L} = \frac{d}{4L}. \tag{6}$$

The most usual way of expressing the dependence between the cylindric sample's elastic modulus on the SF in compressive tests is [4].

$$E_s(S) = E(1 + \beta S^n), \tag{7}$$

where E_s refers to the sample compressive modulus, β is a parameter reported to be near 2 for rubbery materials and the exponent n is reported to be also close to 2 [4]. It is worth to be noted that according to Eq. (7), $E_s(S \rightarrow 0) = E$, meaning long (rod-like) samples lead to more accurate results.

As with compressive tests, existing evidence suggests that the experimentally measured shear modulus is influenced by the geometry of the tested sample. While there is not an available model to directly determine the material's shear modulus from the measured value. Preliminary findings, such as those by Borin et al. in Ref. [19], indicate that samples with higher length and therefore lower SFs produce more accurate results.

3. Materials and methods

This section outlines the preparation of samples of the studied material, the equipment and the experimental methods employed.

3.1. Sample preparation

The material studied is a commercially available room temperature vulcanization (RTV) silicone rubber supplied by WACKER, known as ELASTOSIL® M 4644 A/B [24]. This two-component silicone rubber vulcanizes at room temperature when its two components (A and B) are mixed in a 10:1 wt ratio. The glassy transition temperature of the vulcanized silicone rubber has been determined to be $T_g \leq -50$ °C [3], therefore, at room temperature the material is in its rubbery region.

To achieve a wide range of sample geometries, five molds were fabricated from polymethyl methacrylate (PMMA) sheets of varying thicknesses (1, 2, 3, 5, and 10 mm) using a ROLAND MDX-40A [25] 3D milling machine (see Fig. 2 (a)). Each mold contains cylindrical holes with diameters of 5, 10, 15, and 20 mm (Fig. 2 (b)). This combination of sheet thicknesses and hole diameters results in a total of 20 unique nominal sample sizes, allowing for comprehensive testing across a broad range of geometries as shown in Fig. 3, where the sample sizes prepared are indicated with circle markers demonstrating a homogeneous distribution of samples in terms of their shape factor, represented as a contour plot.

In the preparation process, it is crucial to eliminate any air bubbles in the material, as these can impact the measured properties of the sample. To achieve this, component A is placed in a vacuum chamber (see Fig. 2 (c)) and subjected to vacuum cycles until no air bubbles remain. Next, component B is added in a 10:1 (A:B) weight ratio, and the two components are thoroughly mixed with a glass rod. This mixing step introduces additional air bubbles, necessitating further vacuum cycles to remove them. Once the air bubbles are significantly reduced, and within

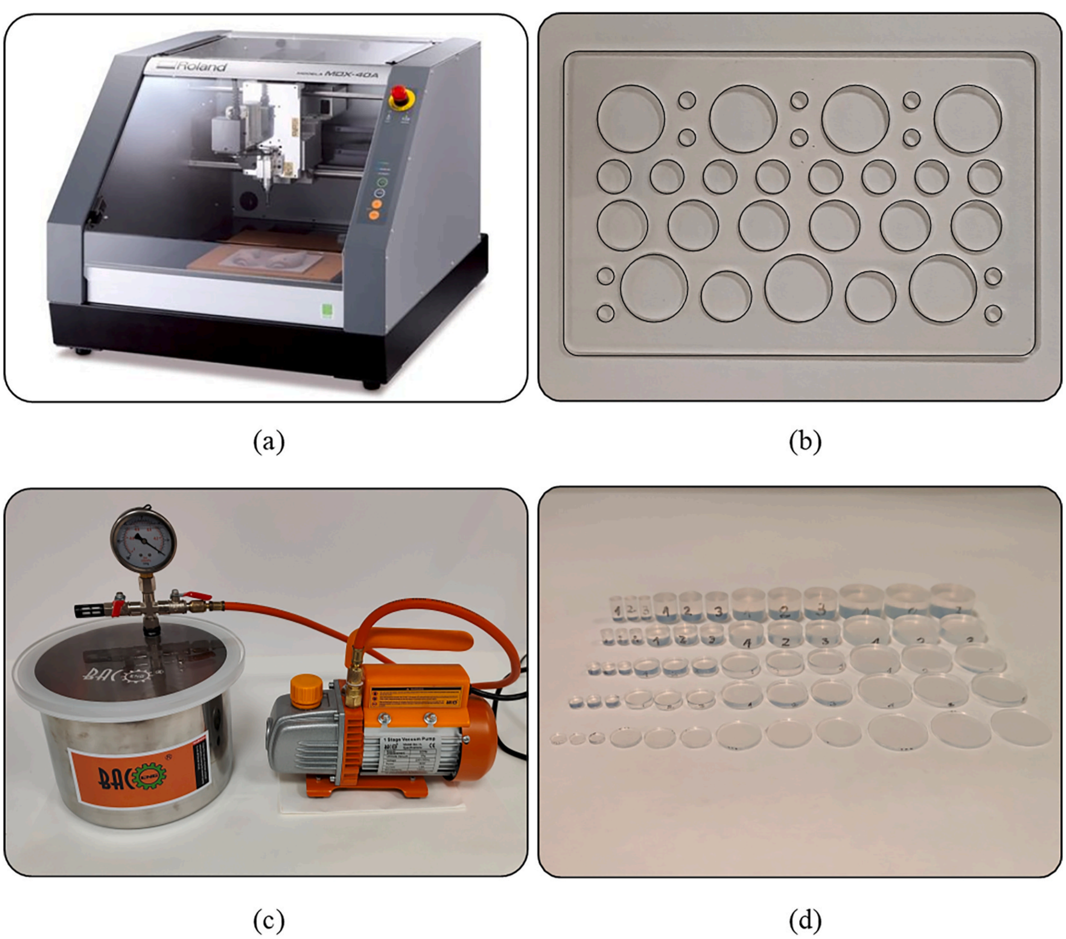

Fig. 2. Equipment and materials used for the preparation of silicone rubber samples: (a) ROLAND MDX-40A 3D milling machine; (b) cylindrical mold made of PMMA; (c) vacuum chamber and pump and (d) silicone rubber samples of various sizes.

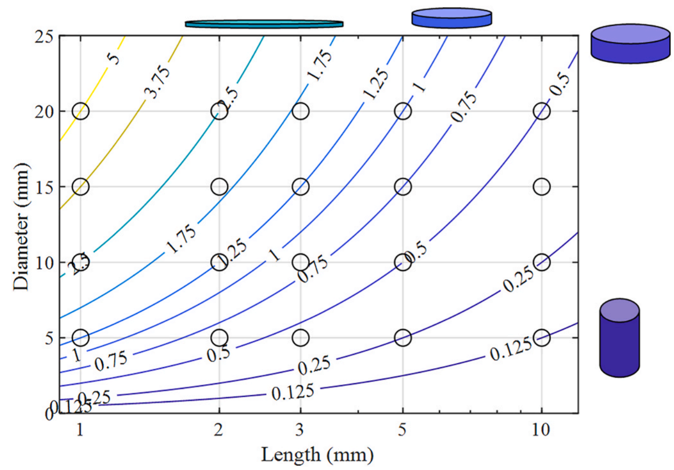

Fig. 3. Contour plot of iso-SF lines as a function of sample diameter (vertical axis) and length (horizontal axis, logarithmic scale). The circle markers indicate the sample sizes used in the experimental study. The surrounding illustrations depict representative sample geometries corresponding to different shape factor regions.

half an hour after mixing, the silicone rubber is poured into the cylindrical molds.

To ensure the molded mixture is bubble-free, additional vacuum cycles are applied. When no bubbles are visible, the upper part of the mold is secured with clamps. After 24 h, vulcanization is complete, and the samples can be demolded. For each nominal size, three different samples are selected, for a total of 60 samples shown in Fig. 2 (d).

3.2. Equipment and experimental methods

The objective of this work includes experimentally measuring the compressive and shear moduli of cylindrical silicone rubber samples. To ensure repeatability, 3 different samples of the same nominal size are tested for 20 different nominal sizes, leading to 60 experiments in total.

On the one hand, to measure the compressive modulus, quasistatic strain ramps are performed using a Dynamic Mechanical Analyzer (DMA) equipped with a compression clamp, specifically, the DMA Q800 model fabricated by T.A. Instruments (Fig. 4 (a)). This equipment can generate force-controlled displacements with a range from 0.001 N to 18 N and measure displacements with 1 nm resolution. The compressive test consists of strain ramps with constant strain-rate $\dot{\varepsilon} = 0.2\ \%/\text{min}$ up to $\varepsilon_{\max} = 1\ \%$ maximum strain to ensure an elastic linear behavior of the material. The tests are performed at room temperature (25 °C ± 2 °C). From the experimental results of the strain ramp, the stress-strain curve of each sample is obtained, from which the compressive modulus of the samples can be determined.

On the other hand, to measure the shear modulus, quasistatic shear strain ramp are performed using the Anton Paar Modular Compact Rheometer (MCR) 302e with a parallel plate configuration (Fig. 4 (b)). This rheometer can exert axial compressive forces up to 50 N and 230 mN m maximum torque and measure angular displacements with a resolution of 0.05 μrad. The shear strain ramps are performed with $\dot{\gamma} = 0.2\ \%/\text{min}$ constant shear strain-rate and $\gamma_{\max} = 1\ \%$ maximum shear strain to ensure an elastic linear behavior of the material. To ensure full contact between the parallel plates and the surface of the samples, $\varepsilon_0 = 2\ \%$ pre-deformation is applied in the axial direction. The tests are performed at room temperature (25 °C ± 2 °C). From the shear strain ramp, the shear stress-strain curves for each prepared sample are obtained from which the sample's shear modulus can be determined.

4. Experimental results

This section shows the experimental results obtained for both the compressive and torsion tests. In each experiment, three samples of the same nominal size are tested to ensure repeatability. From the experimental results, the sample's compressive and shear moduli are obtained by performing a linear regression.

4.1. Sample compressive modulus obtention

The sample compressive modulus E_s is determined through compressive tests conducted on a DMA. Fig. 5 shows the experimental results of the compressive tests.

The results in Fig. 5 show straight stress-strain curves, indicating a linear elastic behavior for the strain range tested. Moreover, the dispersion between samples of the same nominal size is negligible, indicating good repeatability of the tests. In addition, compressive modulus (slope of the curves) increases for samples with greater SFs, which is in accordance with the literature. It can be noted that the strain ramp results of some of the samples are missing. Because of the 18 N force limit of the DMA used for this experiment and the increase in the sample compressive modulus for greater SFs, thinner and wider samples cannot be tested to a significant strain range.

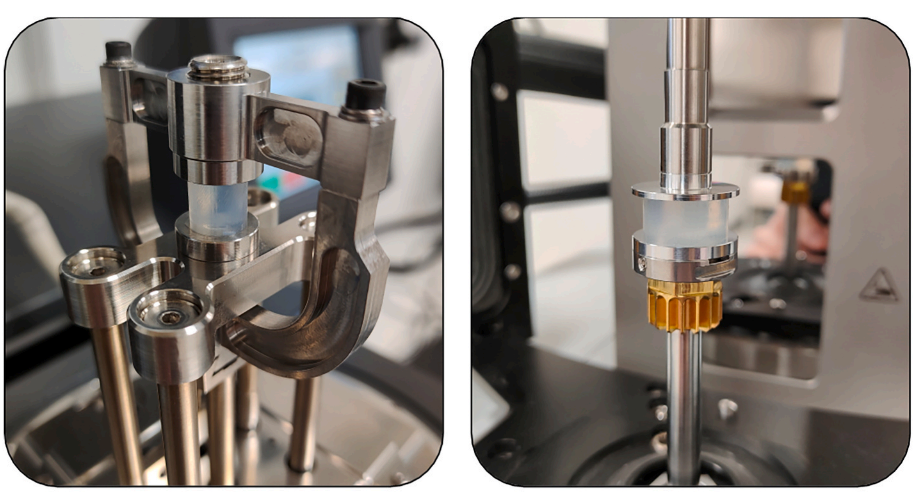

(a) (b)

Fig. 4. Experimental equipment used for characterization: (a) Dynamic mechanical analyzer (DMA) equipped with a compression clamp and (b) rheometer in a parallel plate configuration.

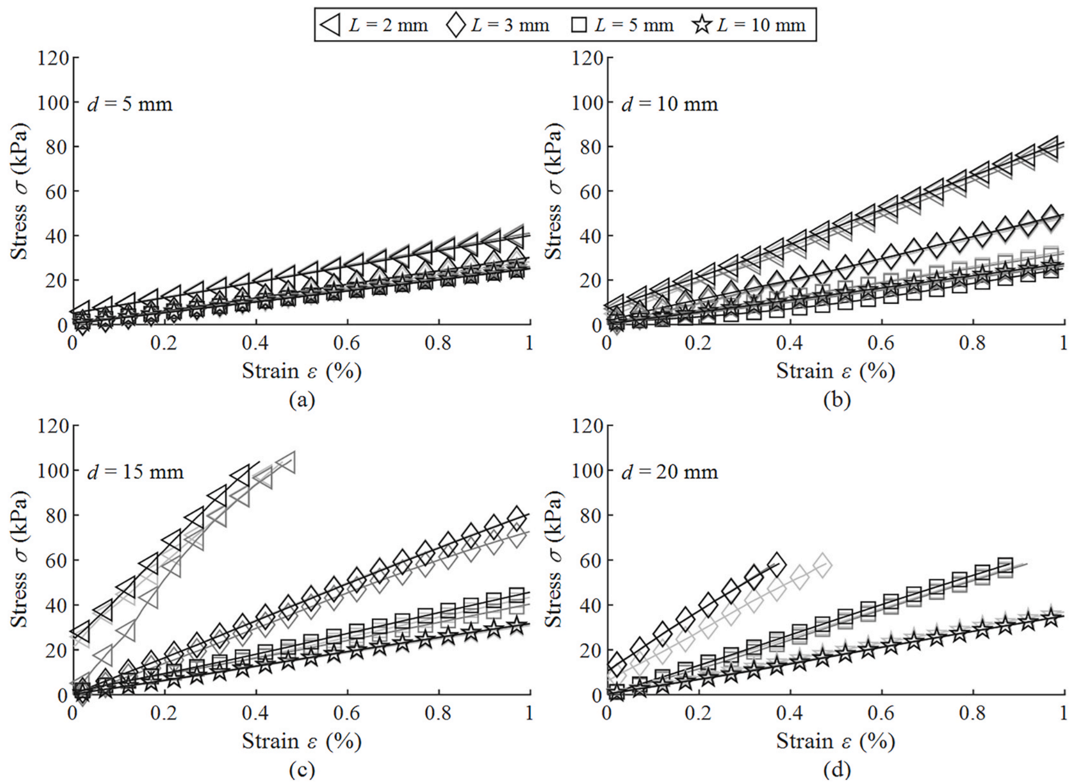

Fig. 5. Stress-strain curves from compressive tests conducted on cylindrical silicone rubber samples. Each curve represents a specific sample nominal length L, indicated by different markers as shown in the legend. Samples of the same nominal size are differentiated by varying grayscale tones. The plots correspond to samples with nominal diameters of (a) $d = 5$ mm, (b) $d = 10$ mm, (c) $d = 15$ mm and (d) $d = 20$ mm.

To evaluate how compressive modulus varies with the SF, a linear regression of each stress-strain curve is performed. Fig. 6 presents the results of the linear regression performed on the compressive stress-strain curves. This figure demonstrates a clear increase in the measured compressive modulus with increasing SF, along with relatively low dispersion among samples of the same nominal size, particularly for those with lower SF values. However, the three data points corresponding to the highest SF values exhibit significant deviations in both dispersion and trend compared to the rest of the data. This can be expected given high SF samples lead to forces and displacements near the range limits of the equipment. Moreover, irregularities in the length of the samples are expected to have a greater relative effect on shorter samples.

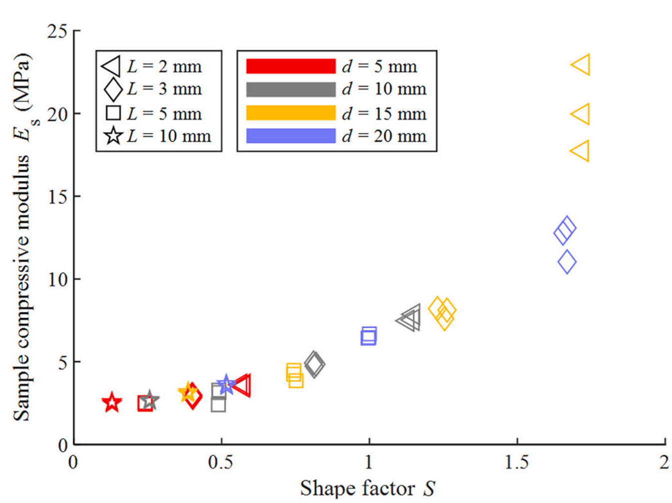

Fig. 6. Compressive modulus of cylindrical silicone rubber samples as a function of the shape factor, obtained through linear regression of the stress-strain data shown in Fig. 3. Each data point corresponds to a specific combination of sample nominal length L and diameter d, with markers representing the lengths and colors indicating the diameters.

Except for the previously mentioned data points, the compressive modulus for samples with the largest SF is found to be approximately four times greater than that for samples with the smallest SF. These results highlight the significant influence of sample geometry on the experimentally obtained compressive modulus.

4.2. Sample shear modulus obtention

The sample shear modulus G_s is determined through torsion tests performed using a rheometer in a parallel plate configuration. Fig. 7 shows the experimental results of the torsion tests for each of the samples.

The shear stress-strain curves in Fig. 7 are straight, indicating a linear elastic behavior of the material within the shear strain range tested. The data shows negligible dispersion between samples of the same nominal size, indicating good repeatability of the tests. Furthermore, the low dispersion observed between samples of different nominal sizes suggests that sample size has a minimal influence on the results. However, the test performed to the samples with nominal size $L = 1$ mm and $d = 20$ mm deviate significantly from the overall trend, exhibiting much greater dispersion. This discrepancy can be attributed to the fact that samples with shorter lengths and larger diameters require less angular displacement and higher torques to achieve the same shear strain and stress, leading to higher relative experimental errors. Additionally, possible irregularities in the length of the samples are likely to have a more pronounced effect on shorter and wider samples [19].

The sample shear modulus was determined by performing a linear regression on each of the experimental shear stress-strain curves. Fig. 8 presents the results of these regressions, with different markers

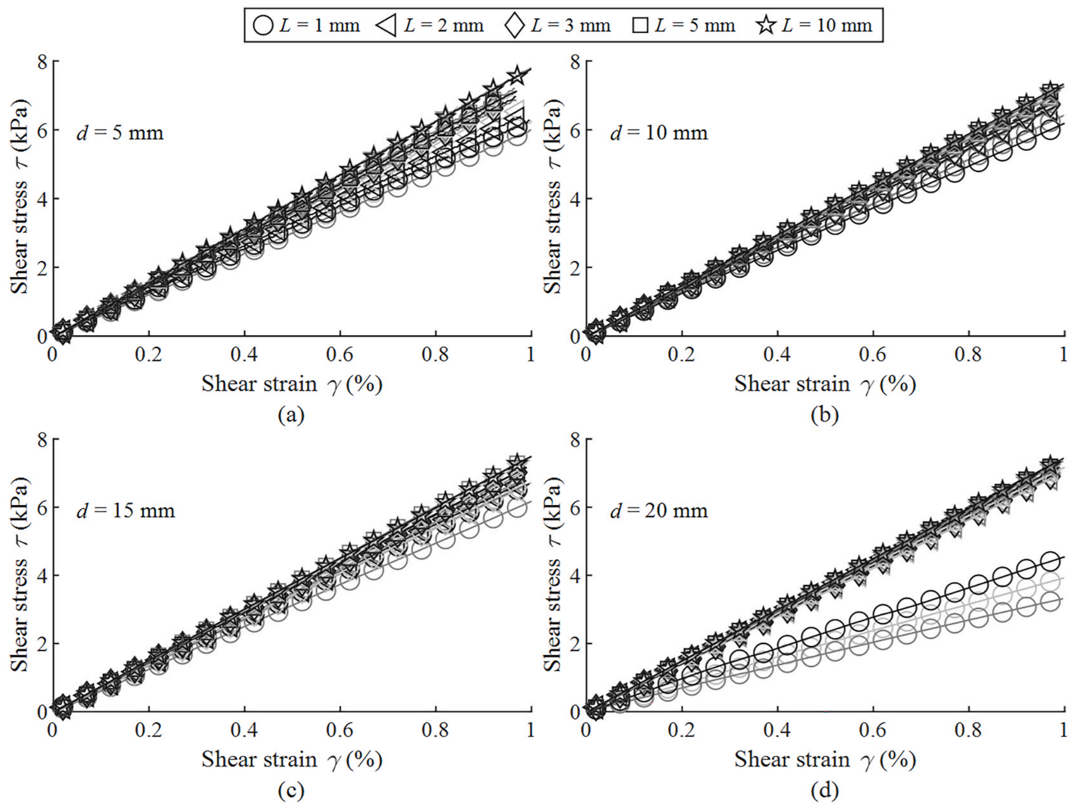

Fig. 7. Shear stress-strain curves from torsion tests conducted on cylindrical silicone rubber samples. Each curve represents a specific sample nominal length L, indicated by different markers as shown in the legend. Samples of the same nominal size are differentiated by varying grayscale tones. The plots correspond to samples with nominal diameters of (a) $d = 5$ mm, (b) $d = 10$ mm, (c) $d = 15$ mm and (d) $d = 20$ mm.

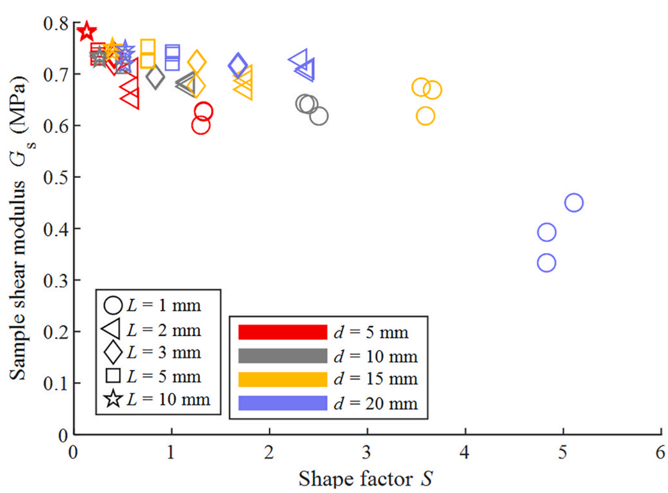

Fig. 8. Shear modulus of cylindrical silicone rubber samples as a function of the shape factor, obtained through linear regression of the shear stress-strain data shown in Fig. 6. Each data point corresponds to a specific combination of sample nominal length L and diameter d, with markers representing the lengths and colors indicating the diameters.

representing the nominal lengths of the samples and different colors indicating their diameters.

Fig. 8 shows a slightly decreasing trend in the measured shear modulus with increasing SF, accompanied by relatively low dispersion among samples of the same nominal size (less than 5 %), particularly for those with lower SF values. However, as previously noted, the last three data points, corresponding to samples with the highest SF, deviate significantly from the observed trend.

Compared to the results from the compressive tests, the variation in the sample shear modulus with the SF is considerably smaller, with a difference of approximately 25 % between the highest and lowest values.

The results obtained in this study are consistent with those reported by Borin et al. in Ref. [19], showing a higher shear modulus and lower dispersion in longer, thinner samples. These findings confirm that testing samples with lower SFs generally yields more reliable and accurate results.

4.3. Sample Poisson's ratio

After the determination of the compressive and shear moduli of each sample, Poisson's ratio can be obtained using Eq. (5). Fig. 9 shows sample Poisson's ratio as a function of their SFs. It needs to be noted that because the compressive modulus of some samples cannot be measured, Poisson's ratio of those samples cannot be determined (see Section 4.1).

The Poisson's ratio values presented in Fig. 9 highlight a recurring issue reported in the literature: although the maximum Poisson's ratio for an isotropic material is 0.5, none of the obtained values remain within this limit. Instead, Poisson's ratio increases with larger shape factors. Notably, a clear trend can be observed in Fig. 9, resembling the behavior of the compressive modulus of the samples, but with a more pronounced rate of change due to the influence of the decreasing shear modulus.

Ignoring the last three data points (given their deviation from the trend of the rest), the highest Poisson's ratio is approximately 16 times greater than the lowest. This indicates an approximately four times higher rate of change than the compressive modulus (Fig. 6) within the same shape factor range. The most extreme values correspond to disk-like samples, where the discrepancy becomes particularly pronounced. This suggests that as the sample geometry deviates further from a

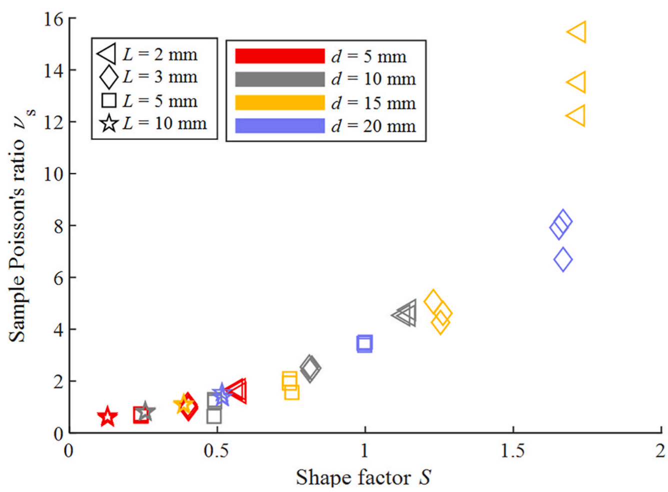

Fig. 9. Poisson's ratio of each sample obtained from the measured sample compressive and shear moduli as a function of the SF. Each data point corresponds to a specific sample nominal length L and diameter d, with markers representing the lengths and colors denoting the diameters.

cylindrical rod-like form and approaches a thin disk, the measured Poisson's ratio becomes increasingly unrealistic, highlighting the strong influence of sample shape on the accuracy of the results.

These results highlight the importance of a correction model for both the compressive and shear moduli to be able to determine Poisson's ratio from the results of compressive and torsion tests.

5. Analysis and modelling of the sample geometry effect

In this section, a mathematical model is proposed to address the effects of sample SF in the elastic properties of the material. The model for the compressive modulus is taken from the literature [4] and is described by Eq. (7), while the models for the shear modulus and Poisson's ratio are proposed phenomenological models to explain the experimental data.

5.1. Proposed mathematical geometry-dependent model

The dependence of cylindrical samples' compressive modulus on their geometry has already been studied [4,5]. In this work, Eq. (7) is used to account for that effect. However, neither the shear modulus nor the Poisson's ratio have been modeled in terms of the SF of the measured samples. Therefore, a phenomenological model is proposed in this work.

On the one hand, the experimental data shown in Fig. 8 suggests that the shear modulus must have a finite value both for small and high SFs. In addition, the proposed function must have a horizontal asymptotic behavior when $S\rightarrow 0$, as suggested by the results in Ref. [19]. On the other hand, Poisson's ratio data shows a very similar tendency to the compressive modulus, but with a higher rate of change within the same SF range. Lastly, Eq. (5) must hold for any proposed model. Everything considered, the proposed phenomenological model for the shear modulus is

$$G_s(S) = G\frac{1+\beta S^n}{1+\alpha S^n}, \tag{8}$$

and substituting Eqs. (7) and (8) in Eq. (5), the resultant sample Poisson's ratio is

$$\nu_s(S) = \nu + \frac{E}{2G}\alpha S^n, \tag{9}$$

where $G = G_s(S\rightarrow 0)$ and $\nu = \nu_s(S\rightarrow 0)$ represent the shear modulus and Poisson's ratio of the material, which is obtained when the SF of the sample tends to zero, i.e. when the sample is 'more rod-like' [19], and α is a model parameter. Notably, the relationship between α and β is critical in determining the behavior of the sample shear modulus G_s as a function of S. When $\alpha > \beta$, the denominator in the G_s model grows faster than the numerator, leading to a decreasing G_s with increasing S, which is expected according to the experimental data. If $\alpha = \beta$, the SF dependency cancels out, resulting in a constant $G_s(S) = G$, indicating that the shear modulus is independent of S, which would suggest minimal geometric influence. Conversely, when $\alpha < \beta$, the numerator grows faster, causing G_s to increase with S, which would contradict the obtained experimental results. In addition, ν_s is independent of β, therefore, the relative value between these two parameters does not affect the behavior of the $\nu_s(S)$ function.

In summary, the proposed model includes six parameters: E, G, ν, β, α and n. However, since E, G, and ν are interrelated through Eq. (5), only five of these parameters are independent.

5.2. Parameter identification via curve fitting

Given $E_s(S)$ and $G_s(S)$, as defined in Eqs. (7) and (8), share the parameters β and n, the curve fitting of the models is done simultaneously. To this end, the function '*fmincon*' of MATLAB R2024b is used, defining as the objective function the following:

$$g(\mathbf{X}) = \frac{1}{N}\sum_i\left(\frac{E_{\mathrm{exp},i} - E_s(S_i,\mathbf{X})}{\max(E_{\mathrm{exp}})}\right)^2 + \frac{1}{M}\sum_j\left(\frac{G_{\mathrm{exp},j} - G_s(S_j,\mathbf{X})}{\max(G_{\mathrm{exp}})}\right)^2, \tag{10}$$

where $\mathbf{X} = (E, G, \beta, \alpha, n)$ is a vector containing the model parameters, N and M are the total number of experimental data points for the sample compressive and shear modulus respectively, $E_{\mathrm{exp},i}$ is the i-th sample compressive modulus obtained experimentally, S_i is the shape factor of the i-th sample, $G_{\mathrm{exp},j}$ is the j-th sample shear modulus obtained experimentally and S_j is the shape factor of the j-th sample. The only constraint applied to the parameter values is that all of them must be positive. In addition, the experimental data points marked by red asterisks (*) in Fig. 10 where not considered for the curve fitting process given their deviation from the trend of the rest of the data points.

The last evaluation of the objective function is $g(\mathbf{X}_{\mathrm{last}}) = 2.33\times 10^{-3}$. In Fig. 10, the resultant models along with the experimental data for both the compressive and shear moduli are shown.

Fig. 10 (a) shows the result of the model curve fitting for the compressive modulus. The model effectively captures the variability of the experimental data, with a coefficient of determination $(R^2)_E = 0.982$. The results for the fitted parameters indicate that the compressive modulus of the studied material is $E = 2.26$ MPa which is an expectable value for a silicone rubber [26]. Moreover, the parameters $\beta = 1.75$ and $n = 1.85$ stay close to their expected value of 2 (see Section 2).

Fig. 10 (b) shows the result of the model curve fitting for the shear modulus of the material. In this case the coefficient of determination is lower, with a value of $(R^2)_G = 0.463$. This lower value can be explained by the fact that the ratio of the total data variation to dispersion is much lower in this case. However, the model shows good accordance with the experimental data. The fitted parameters show that the shear modulus of the material is $G = 0.763$ MPa with a model parameter $\alpha = 2.01$ which is greater than β indicating a decreasing trend in G_s as mentioned in Section 5.1.

5.3. Model validation: Poisson's ratio determination

From the fitted value of the compressive and shear models parameters and using Eq. (9), Poisson's ratio model can be obtained. In Fig. 11, the obtained model is compared to the experimental data. The model shows a high coefficient of determination $(R^2)_\nu = 0.977$, indicating that accurately captures the trend of the experimental data. It is worth noting

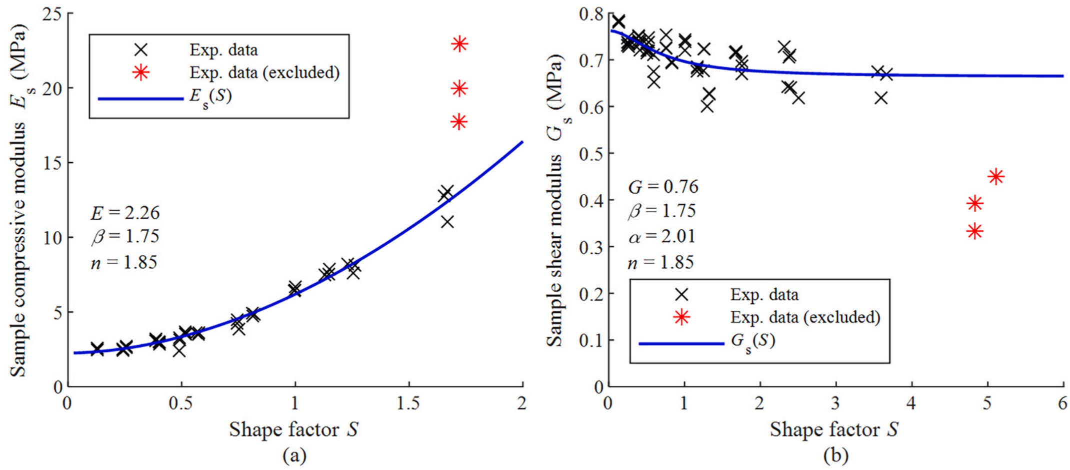

Fig. 10. Curve fitting results for the compressive and shear modulus models. The blue solid lines represent the fitted models: (a) the compressive modulus model, and (b) the shear modulus model. Experimental data points (×) are included in the fitting process, while excluded data points (*) are indicated separately.

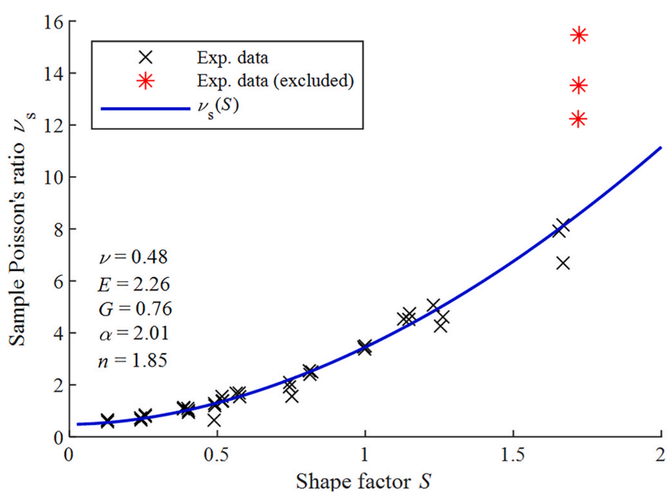

Fig. 11. Resultant model for the sample Poisson's ratio as a function of the shape factor. The blue solid line represents the model derived from the compressive and shear modulus models. Experimental data points (×) correspond to the Poisson's ratio calculated for each sample. Data points indicated by (*) are excluded from the coefficient of determination calculation.

that the highest SF data points (indicated by (*) marker in Fig. 11) have been excluded for the $(R^2)_\nu$ calculation, as they were also excluded for the curve fitting process in the compressive modulus analysis.

As indicated in Fig. 11, the value obtained for the material's Poisson's ratio is $\nu = 0.48$ which is in great accordance with the value reported in Ref. [9] for silicone rubbers measured via DIC techniques.

6. Conclusions

This study investigated the influence of sample geometry on the quasistatic compressive and shear moduli of a silicone rubber and its impact on the determination of Poisson's ratio. The compressive and shear moduli were experimentally obtained from compression and torsion tests performed on the same cylindrical samples with varying SFs. The results confirmed that the compressive modulus exhibits a strong dependency on SF, increasing significantly with larger values, while the shear modulus also shows a dependency, but to a lesser extent. Consequently, Poisson's ratio, when calculated directly from these uncorrected measurements, exceeds the theoretical limit of 0.5.

To account for these geometric effects, a mathematical model was proposed to describe the dependency of both the shear modulus and Poisson's ratio on the SF. The model extends an existing correction for the compressive modulus by introducing a phenomenological equation for the shear modulus. The model was validated through experimental data fitting of the compressive and shear moduli, and Poisson's ratio model was obtained from the other two. The corrected value of Poisson's ratio ($\nu = 0.48$) aligns with the expected results for an incompressible silicone rubber, demonstrating the model's ability to account for geometric effects in both compressive and torsion tests.

The findings of this study emphasize the importance of considering geometric influences when characterizing elastomers through compressive and torsion tests, as neglecting these effects leads to significant errors in the elastic and shear moduli and Poisson's ratio estimations. The proposed approach provides a practical and reliable means of obtaining corrected values for these properties, enhancing the accuracy of material characterization.

CRediT authorship contribution statement

Julen Cortazar-Noguerol: Writing – original draft, Visualization, Validation, Software, Methodology, Investigation, Formal analysis, Data curation, Conceptualization. **Fernando Cortés:** Writing – review & editing, Supervision, Project administration, Methodology, Formal analysis, Conceptualization. **Iker Agirre-Olabide:** Writing – review & editing, Supervision, Methodology. **María Jesús Elejabarrieta:** Writing – review & editing, Supervision, Project administration, Methodology, Funding acquisition, Formal analysis, Conceptualization.

Declaration of generative AI and AI-assisted technologies in the Writing process

During the preparation of this work the authors used ChatGPT-4o to improve the readability and language of the manuscript. After using this tool, the authors reviewed and edited the content as needed and take full responsibility for the content of the published article.

Declaration of competing interest

The authors declare that they have no known competing financial interests or personal relationships that could have appeared to influence the work reported in this paper.

Acknowledgements

This research has been supported by the University of Deusto

Research Training Grants Program (grant reference number FPI UD_2023_07) and the Department of Education for the Research Group program IT1507-22.

Data availability

Data will be made available on request.

References

[1] J.B. Pascual-Francisco, L.I. Farfan-Cabrera, O. Susarrey-Huerta, Characterization of tension set behavior of a silicone rubber at different loads and temperatures via digital image correlation, Polym. Test. 81 (2020) 106226, https://doi.org/10.1016/j.polymertesting.2019.106226.
[2] L.I. Farfan-Cabrera, J.B. Pascual-Francisco, An experimental methodological approach for obtaining viscoelastic Poisson's ratio of elastomers from creep strain DIC-based measurements, Exp. Mech. 62 (2022) 287–297, https://doi.org/10.1007/s11340-021-00792-9.
[3] I. Agirre-Olabide, M.J. Elejabarrieta, Maximum attenuation variability of isotropic magnetosensitive elastomers, Polym. Test. 54 (2016) 104–113, https://doi.org/10.1016/j.polymertesting.2016.06.021.
[4] R.P. Brown, Physical Testing of Rubber, Springer Netherlands, Dordrecht, 1996, https://doi.org/10.1007/978-94-011-0529-3.
[5] ISO 7743:2017 Rubber, Vulcanized or Thermoplastic — Determination of Compression Stress-Strain Properties. ISO; n.d.
[6] B.A. Szabó, I. Babuška, Finite Element Analysis: Method, Verification and Validation, second ed., Wiley, Hoboken, NJ, 2021.
[7] H.W. Smith, R.E. Chapel, Poisson's ratio determined with strain rosettes, Exp. Mech. 9 (1969) 140–141, https://doi.org/10.1007/BF02327701.
[8] Z. Laufer, Y. Diamant, M. Gill, G. Fortuna, A simple dilatometric method for determining Poisson's ratio of nearly incompressible elastomers, Int. J. Polym. Mater. Polym. Biomater. 6 (1978) 159–174, https://doi.org/10.1080/00914037808077906.
[9] J.A. Sotomayor-del-Moral, J.B. Pascual-Francisco, O. Susarrey-Huerta, C. D. Resendiz-Calderon, E.A. Gallardo-Hernández, L.I. Farfan-Cabrera, Characterization of viscoelastic Poisson's ratio of engineering elastomers via DIC-based creep testing, Polymers 14 (2022) 1837, https://doi.org/10.3390/polym14091837.
[10] S. Dogru, B. Aksoy, H. Bayraktar, B.E. Alaca, Poisson's ratio of PDMS thin films, Polym. Test. 69 (2018) 375–384, https://doi.org/10.1016/j.polymertesting.2018.05.044.
[11] A.V. Boiko, V.M. Kulik, B.M. Seoudi, H.H. Chun, I. Lee, Measurement method of complex viscoelastic material properties, Int. J. Solid Struct. 47 (2010) 374–382, https://doi.org/10.1016/j.ijsolstr.2009.09.037.
[12] H. Vatandoost, M. Hemmatian, R. Sedaghati, S. Rakheja, Effect of shape factor on compression mode dynamic properties of magnetorheological elastomers, J. Intell. Mater. Syst. Struct. 32 (2021) 1678–1699, https://doi.org/10.1177/1045389X20983921.
[13] A. Yaghoobi, A. Jalali, M. Norouzi, M. Ghatee, Aspect ratio dependency of magneto-rheological elastomers in dynamic tension-compression loading, IEEE Trans. Magn. 58 (2022) 1–13, https://doi.org/10.1109/TMAG.2022.3152031.
[14] C. Dessi, G.D. Tsibidis, D. Vlassopoulos, M. De Corato, M. Trofa, G. D'Avino, et al., Analysis of dynamic mechanical response in torsion, J. Rheol. 60 (2016) 275–287, https://doi.org/10.1122/1.4941603.
[15] S. Pal, A. Bhattacharyya, Measurement of axial and shear mechanical response of PDMS elastomers and determination of Poisson's ratio using digital image correlation, Polym. Test. 143 (2025) 108687, https://doi.org/10.1016/j.polymertesting.2025.108687.
[16] I. Agirre-Olabide, J. Berasategui, M.J. Elejabarrieta, M.M. Bou-Ali, Characterization of the linear viscoelastic region of magnetorheological elastomers, J. Intell. Mater. Syst. Struct. 25 (2014) 2074–2081, https://doi.org/10.1177/1045389X13517310.
[17] I. Agirre-Olabide, M. Jesus Elejabarrieta, Effect of synthesis variables on viscoelastic properties of elastomers filled with carbonyl iron powder, J. Polym. Res. 24 (2017) 139, https://doi.org/10.1007/s10965-017-1299-z.
[18] ISO 3219-2:2022 Rheology - Part 2: General Principles of Rotational and Oscillatory Rheometry. ISO; n.d.
[19] D. Borin, N. Kolsch, G. Stepanov, S. Odenbach, On the oscillating shear rheometry of magnetorheological elastomers, Rheol. Acta 57 (2018) 217–227, https://doi.org/10.1007/s00397-018-1071-2.
[20] B.L. Walter, J.-P. Pelteret, J. Kaschta, D.W. Schubert, P. Steinmann, On the wall slip phenomenon of elastomers in oscillatory shear measurements using parallel-plate rotational rheometry: I. Detecting wall slip, Polym. Test. 61 (2017) 430–440, https://doi.org/10.1016/j.polymertesting.2017.05.035.
[21] B.L. Walter, J.-P. Pelteret, J. Kaschta, D.W. Schubert, P. Steinmann, On the wall slip phenomenon of elastomers in oscillatory shear measurements using parallel-plate rotational rheometry: II. Influence of experimental conditions, Polym. Test. 61 (2017) 455–463, https://doi.org/10.1016/j.polymertesting.2017.05.036.
[22] M. Sheidaei, A. Gudmarsson, M. Langfjell, Effect of various dynamic shear rheometer testing methods on the measured rheological properties of bitumen, Materials 16 (2023) 2745, https://doi.org/10.3390/ma16072745.
[23] M.-A. Keip, M. Rambausek, Computational and analytical investigations of shape effects in the experimental characterization of magnetorheological elastomers, Int. J. Solid Struct. 121 (2017) 1–20, https://doi.org/10.1016/j.ijsolstr.2017.04.012.
[24] ELASTOSIL® M 4644 A/B | Room Temperature Curing Silicone Rubber (RTV-2) | Wacker Chemie AG. WACKER Website n.d. https://www.wacker.com/h/en-us/c/elastosil-m-4644-ab/p/000005351 (accessed February 6, 2025).
[25] Modela MDX-40A 3D Milling Machine | Roland DGA. Roland Website n.d. https://www.rolanddga.com/es-la/soporte/products/milling/modela-mdx-40a-3d-milling-machine (accessed February 6, 2025).
[26] Overview of materials for Silicone Rubber n.d. https://www.matweb.com/search/datasheet.aspx?MatGUID=cbe7a469897a47eda563816c86a73520 (accessed January 30, 2025).